Ground state in the novel dimer iridate $Ba_{13}Ir_6O_{30}$ with $Ir^{6+}(5d^3)$ ions

Hengdi Zhao,[1] Feng Ye,[2] Hao Zheng,[1] Bing Hu,[1,3] Yifei Ni,[1] Yu Zhang,[1] Itamar Kimchi,[1,4] and Gang Cao[1,*]

[1]*Department of Physics, University of Colorado, Boulder, Colorado 80309, USA*

[2]*Neutron Scattering Division, Oak Ridge National Laboratory, Oak Ridge, Tennessee 37831, USA*

[3]*School of Mathematics and Physics, North China Electric Power University, Beijing 102206, China*

[4]*JILA, NIST and Department of Physics, University of Colorado, Boulder, Colorado 80309, USA*

(Received 9 May 2019; revised manuscript received 5 July 2019; published 23 August 2019)

We have synthesized and studied an iridate, $Ba_{13}Ir_6O_{30}$, with unusual Ir oxidation states: 2/3 $Ir^{6+}(5d^3)$ ions and 1/3 $Ir^{5+}(5d^4)$ ions. Its crystal structure features dimers of face-sharing IrO_6 octahedra, and IrO_6 monomers that are linked via long, zigzag Ir-O-Ba-O-Ir pathways. Nevertheless, $Ba_{13}Ir_6O_{30}$ exhibits two transitions at $T_{N1} = 4.7$K and $T_{N2} = 1.6$ K. This magnetic order is accompanied by a huge Sommerfeld coefficient 200 mJ/mole K^2 below T_{N2}, signaling a coexisting frustrated/disordered state persisting down to at least 0.05 K. This iridate hosts unusually large $J_{\text{eff}} = 3/2$ degrees of freedom, which is enabled by strong spin-orbit interactions (SOI) in the monomers with Ir^{6+} ions and a joint effect of molecular orbitals and SOI in the dimers occupied by Ir^{5+} and Ir^{6+} ions. Features displayed by the magnetization and heat capacity suggest that the combination of covalency, SOI, and large effective spins leads to highly frustrated ferrimagnetic ordering, an interesting feature of this high-spin iridate.

DOI: 10.1103/PhysRevB.100.064418

I. INTRODUCTION

The inherently strong spin orbit interactions (SOI) in iridates can create an entirely new hierarchy of energy scales and unique competitions between fundamental interactions (e.g., SOI $\sim$ 0.4 eV, Coulomb interaction U $\sim$ 0.5 eV) that result in intriguing consequences, such as the SOI-entangled $J_{\text{eff}} = 1/2$ state [1–8]. In essence, the strong SOI split the broad $5d$ bands into two narrow bands, namely, $J_{\text{eff}} = 1/2$ and $J_{\text{eff}} = 3/2$ bands [1]. The $Ir^{4+}(5d^5)$ ion provides four d electrons to fill the lower $J_{\text{eff}} = 3/2$ bands, and one electron to partially fill the upper $J_{\text{eff}} = 1/2$ band that lies closest to the Fermi energy and dominates underlying physical properties. Indeed, the $J_{\text{eff}} = 1/2$ state with spin $S = 1/2$ and effective orbital moment $L_{\text{eff}} = 1$ is a building block essential to a panoply of phases observed or proposed in recent years [4–8]. The $Ir^{5+}(5d^4)$ ion, on the other hand, provides all four d electrons to fill the lower $J_{\text{eff}} = 3/2$ bands, leaving the upper $J_{\text{eff}} = 1/2$ band empty, thus $S = 1$ and $L_{\text{eff}} = 1$ or a nonmagnetic singlet $J_{\text{eff}} = 0$ state. However, growing evidence indicates magnetic states emerging in pentavalent iridates when exchange interactions (0.05–0.10 eV), singlet-triplet splitting (0.050–0.20 eV), noncubic crystal fields, and SOI are comparable and compete [9–15].

Nevertheless, studies of iridates have almost exclusively focused on tetravalent $Ir^{4+}(5d^5)$ and pentavalent $Ir^{5+}(5d^4)$ iridates thus far. There exist some pioneering studies on hexavalent $Ir^{6+}(5d^3)$ iridates addressing structural and magnetic properties of the iridates [16–26]. However, our knowledge on the physics of hexavalent iridates is conspicuously lacking, in part, because such a high oxidation state is not as common as Ir^{4+} and Ir^{5+} in iridates. A d^3 ion in an octahedron normally generates an $S = 3/2$ state (with the quenched orbital moment $L = 0$) when the Hund's ruling coupling J_{H} is much stronger than SOI. However, for the $Ir^{6+}(5d^3)$ ion, the SOI is almost as strong as that in the $Ir^{4+}(5d^5)$ and $Ir^{5+}(5d^4)$ ions [25]; accordingly, three d electrons in the Ir^{6+} ion fill three of the four orbitals determined by the j-j coupling, forming a SOI-entangled $J_{\text{eff}} = 3/2$ state. The $J_{\text{eff}} = 3/2$ state was recently observed in $Os^{5+}(5d^3)$ based oxides [26]. Furthermore, the overwhelming balance of interest has been given to iridates with either corner-sharing octahedra (e.g., perovskite iridates) or edge-sharing octahedra (e.g., honeycomb iridates). Very limited work on iridates with facing-sharing octahedra has been conducted until very recently [27–32]. It needs to be emphasized that the Ir-Ir bond distance in facing-sharing octahedra ($2/\sqrt{3}\, d_{\text{Ir-O}} \approx 1.16 d_{\text{Ir-O}}$, where $d_{\text{Ir-O}}$ is the Ir-O bond distance in an undistorted octahedron) is shorter than that both in corner-sharing octahedra ($2d_{\text{Ir-O}}$) and edge-sharing octahedra ($\sqrt{2}d_{\text{Ir-O}}$). There is mounting evidence that suggests that the shorter Ir-Ir bond distance facilitates a strong covalency/electron hopping, which, along with the SOI, may significantly alter or diminish the J_{eff} states, resulting in different quantum phases in dimer systems [27–32].

Here we report an exotic magnetic state in a synthesized single-crystal iridate $Ba_{13}Ir_6O_{30}$. This compound, which did not exist previously, to our knowledge, consists of 2/3 hexavalent Ir^{6+} $(5d^3)$ ions and 1/3 pentavalent $Ir^{5+}(5d^4)$ ions, rendering an average oxidation state of $Ir^{+5.67}$. The crystal structure of the compound features two slightly different dimers of face-sharing IrO_6 octahedra and additional IrO_6 monomers. There is no obviously strong connectivity that links the dimers and/or monomers but long, zigzag Ir-O-Ba-O-Ir pathways appear [Fig. 1(a)]. However, $Ba_{13}Ir_6O_{30}$ strikingly exhibits an antiferromagnetic (AFM) transition at $T_{N1} = 4.7$ K and a transition or crossover feature at $T_{N2} =$

*gang.cao@colorado.edu

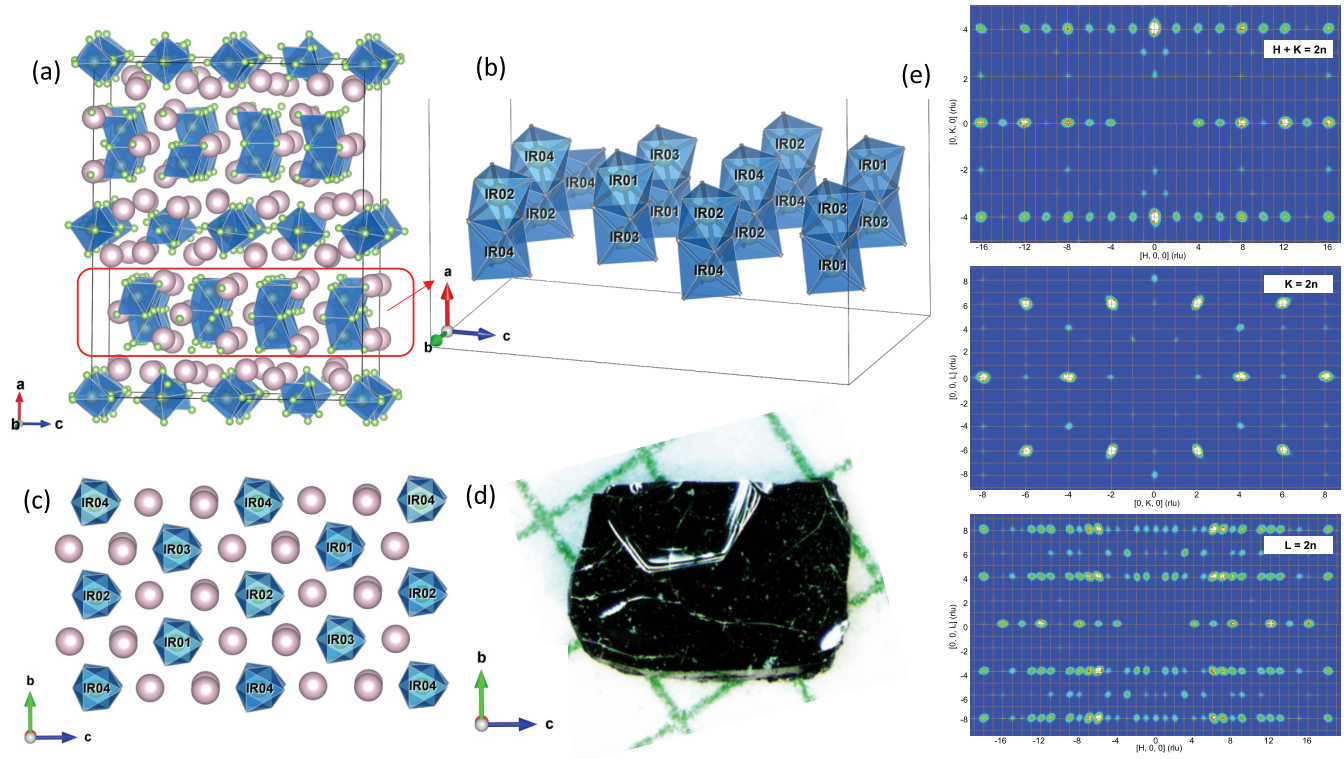

FIG. 1. Crystal structure: (a) The dimers and monomers that are connected via long, zigzag Ir-O-Ba-O-Ir pathways along the c axis. (b) The arrangement of dimers. Note that Ir1-Ir3 and Ir2-Ir4 are the Dimer S and Dimer L, respectively. (c) The bc plane to further illustrate the weak connectivity of the dimers and monomers. (d) An image of a representative single crystal of $Ba_{13}Ir_6O_{30}$ with the bc plane. (e) Three representative images of the reciprocal lattice, which unambiguously reveal the high-quality of the single crystal and the space group (#60). These images are obtained via our neutron diffraction measurements.

1.6 K, respectively, indicating established three-dimensional correlations below T_{N1}. Hysteresis at T_{N1} suggests a nonzero net ferromagnetic moment, i.e., ferrimagnetism or magnetic canting. The average effective moment μ_{eff} is $\sim 4.50\,\mu_B$/f.u. which, as we discuss below, requires at least some of the local moments to be larger than spin-one-half, consistent with Hund's rule coupling ($J_H \sim 0.7$ eV) [28] playing a role constrained by SOI. Interestingly, the T_{N1} net moment μ_s parallel to an applied field is $1.14\,\mu_B$/f.u. and the entropy removal is only $\sim$ 3.7 J/mole K below 5 K. Below T_{N2}, a huge Sommerfeld coefficient $\gamma = 200\,\text{mJ/mole K}^2$ is observed, signaling gapless excitations suggestive of a frustrated/disordered phase persisting down to at least 0.05 K. This behavior is attributed to an incomplete removal of the large spin degrees of freedom unique to $Ba_{13}Ir_6O_{30}$. We argue that an unusual spin-orbit-entangled $J_{\text{eff}} = 3/2$ state is hosted by the monomers with Ir^{6+} ions or monomers^{6+}, while a distinct quasispin state dictated by molecular orbitals is hosted by the dimers with both Ir^{6+} and Ir^{5+} ions. This work, along with comparisons drawn with other dimer iridates, suggests that a combined effect of the strong covalency and SOI suppresses conventional J_{eff} states, leading to the exotic quantum ground state with large residual entropy.

II. RESULTS AND DISCUSSION

$Ba_{13}Ir_6O_{30}$ adopts an orthorhombic structure with a *Pbcn* (No. 60) space group. The lattice parameters at 100 K are $a = 25.4716(7)$, $b = 11.7548(3)$ Å, and $c = 20.5668(6)$ Å, respectively. The unit cell consists of 48 Ir ions (Fig. 1) [see Supplemental Material (SM) for more details [33]]. Since the structure of this compound was never reported before, to our knowledge, an intensive structural study of the single-crystal $Ba_{13}Ir_6O_{30}$ at different temperatures has been conducted using both single-crystal x-ray diffraction and neutron diffraction to ensure an accurate determination of the crystal structure of this compound [33]. The single crystals of $Ba_{13}Ir_6O_3$ are clearly of high quality, as shown in Figs. 1(d) and 1(e).

The first striking feature of $Ba_{13}Ir_6O_{30}$ involves its unusual magnetic oxidation states. $Ba_{13}Ir_6O_{30}$ hosts 2/3 hexavalent Ir^{6+} ($5d^3$) ions and 1/3 pentavalent Ir^{5+}($5d^4$) ions that give rise to an average $Ir^{+5.67}$ oxidation state. There are two slightly different dimers. The Ir1 and Ir3 ions form the shorter dimer or Dimer S and the Ir2 and Ir4 ions form the longer one or Dimer L [Fig. 1(b)]. At 100 K, the Ir1-Ir3 bond distance of the Dimer S(= 2.752 Å) is shorter than the Ir2-Ir4 bond distance of the Dimer L(= 2.789 Å) by 1.3%. Both Dimers L and Dimer S are alternatively arranged along the c axis [Fig. 1(b)]. Each dimer consists of two slightly inequivalent octahedral sites. The IrO_6 monomers are highly distorted but their average Ir-O bond distance fluctuates around 1.92 Å, as expected for Ir^{6+} ions [16]. Thus, all monomers host a hexavalent Ir^{6+}($5d^3$) ion. Each IrO_6 octahedron has a strong trigonal distortion in the dimers. There are eight Dimer S's, eight Dimer L's, and sixteen IrO_6 monomers in a unit cell [33]. It is emphasized that the dimers and monomers are only linked by

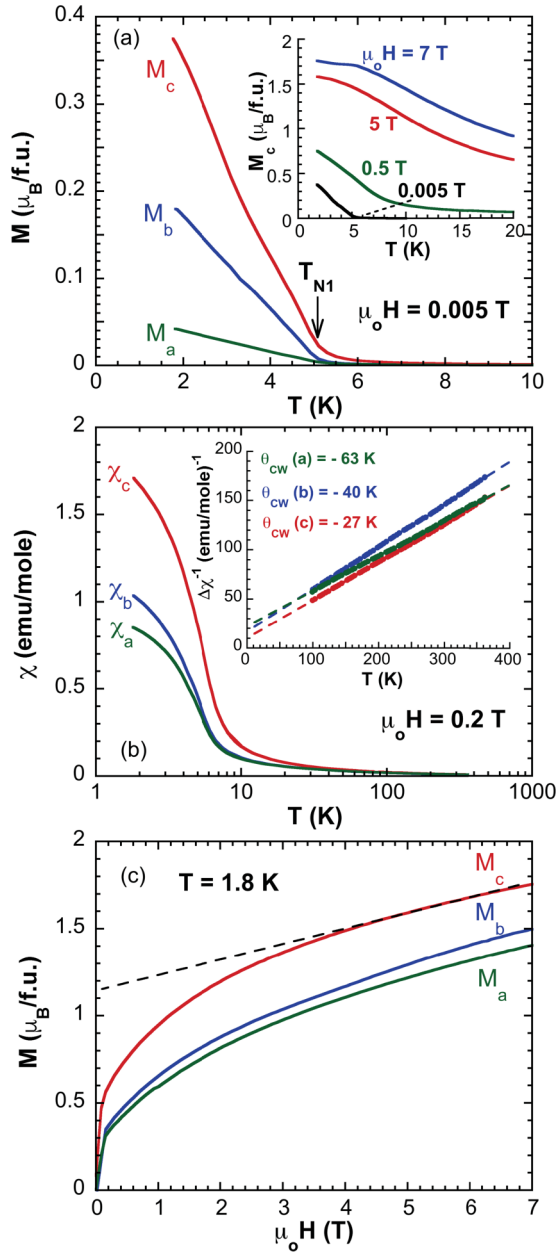

FIG. 2. Magnetic properties: Temperature dependence of (a) the magnetization M for the a-, b-, and c-axis, M_a, M_b, and M_c at $\mu_o H = 0.005$ T. Inset: M_c at various fields; (b) the magnetic susceptibility for the a-, b-, and c axis, χ_a, χ_b, and χ_c at $\mu_o H = 0.2$ T. Inset: the corresponding $\Delta\chi$ vs T. (c) The isothermal magnetization for the a-, b-, and c axis at 1.8 K.

long, zigzag Ir-O-Ba-O-Ir pathways in the bc plane [Figs. 1(a) and 1(c)].

Despite the unfavorable connectivity for three-dimensional correlations, $Ba_{13}Ir_6O_{30}$ undergoes two magnetic transitions below 5 K. The magnetization M for three principal axes exhibits an abrupt rise at $T_{N1} = 4.7$K and anomalous behavior leading to another transition at $T_{N2} = 1.6$ K [see Fig. 2(a), and heat capacity $C(T)$ discussed below]. The observed large magnetic anisotropy indicates that the SOI is significant in spite of the trigonal distortion in the IrO_6 octahedra. The c-axis magnetization M_c is also measured at various fields and exhibits a rounded but still well-defined anomaly near T_{N1} at 7 T [Fig. 2(a) Inset].

Data fits to the Curie-Weiss law yield a Curie-Weiss temperature $\theta_{CW} = -63$, -40, and -27 K for the a, b, and c axis, respectively [Fig. 2(b)]. The negative θ_{CW} conforms to an AFM exchange interaction in the system. The corresponding frustration parameter, defined as $f = |\theta_{CW}|/T_N$, is as large as 13, signaling sizable frustration in the system. The effective moment μ_{eff} is 4.74, 4.29, and 4.56 μ_B/f.u. for the a, b, and c axis, respectively. Given six Ir ions (two Ir^{5+} ions and four Ir^{6+} ions) per formula, these values are inconsistent with those expected for either the Hund's rule physics or the single-site physics of ideal isolated octahedra in which $J_{eff} = 0$ for $Ir^{5+}(5d^4)$ ions and $J_{eff} = 3/2$ for $Ir^{6+}(5d^3)$ ions. Instead, the two AFM transitions and the reduced μ_{eff} imply an existence of strongly coupled Ir pairs or molecular orbitals in this system, further discussed below.

The isothermal magnetization $M(H)$ at 1.8 K exhibits a curvature with increasing H, suggesting a weak ferromagnetic behavior due to magnetic canting or the Dzyaloshinskii–Moriya (DM) interactions below T_{N1} [Fig. 2(c)]. This is consistent with a strong hysteresis effect observed below T_{N1} when the sample is measured in a zero-field cooled and a field cooled sequence, respectively. Extrapolating M_c to $H = 0$ yields an ordered moment of 1.14 μ_B/f.u.

The specific heat $C(T)$ measured down to 0.05 K confirms the existence of long-range magnetic order. $C(T)$ exhibits a sharp anomaly at $T_{N1} = 4.7$ K and a broader feature at $T_{N2} = 1.6$ K [see Fig. 3(a)]. The anomalies are better illustrated in a C/T vs T plot shown in Fig. 3(b). $C(T)$ measured at $\mu_o H = 1$ T shows a discernible increase in both transitions T_{N1} and T_{N2}, and a broadening of T_{N1}. It is important to be pointed out that both T_{N1} and T_{N2} do not show a λ transition expected for a typical second-order phase transition such as the one observed in a related dimer iridate, $Ba_5AlIr_2O_{11}$ [27]. An analysis of the $C(T)$ data yields an entropy removal of approximately 3.70 J/mole K below T_{N1}, significantly smaller than that anticipated for any spin systems. Indeed, the Sommerfeld coefficient or γ extrapolated above T_{N1} and below T_{N2} are 480 and 200 mJ/mole K^2 (or 80 and 33 mJ/Ir mole K^2), respectively [see Fig. 3(c)]. For comparison and contrast, this value is zero for $Ba_5AlIr_2O_{11}$ [27] and $BaIrO_3$ [34] and 17 mJ/mole K^2 (or 6 mJ/Ir mole K^2) for $Ba_4Ir_3O_{10}$ [31]. Such surprisingly huge values of γ, which are conventionally expected in a highly correlated metal, signal a large amount of remaining entropy or an existence of a significantly frustrated/disordered state that persists down to at least 0.05 K coexisting with the ordered magnetic state.

The b-axis electrical resistivity ρ_b between 100 and 800 K exhibits an activation behavior with an activation charge-gap of 0.23 eV (Fig. 4). ρ_b becomes too high for measurements below 100 K and remains an excellent electrical insulator. $Ba_{13}Ir_6O_{30}$ shows no sign of charge order over this wide temperature range, in contrast to $Ba_5AlIr_2O_{11}$ in which a charge order occurs at 210 K [27].

It is clear that three-dimensional magnetic correlations are established at low temperatures, which means that all IrO_6 monomers and dimers must participate in the long-range magnetic order, despite the remarkably weak connectivity between

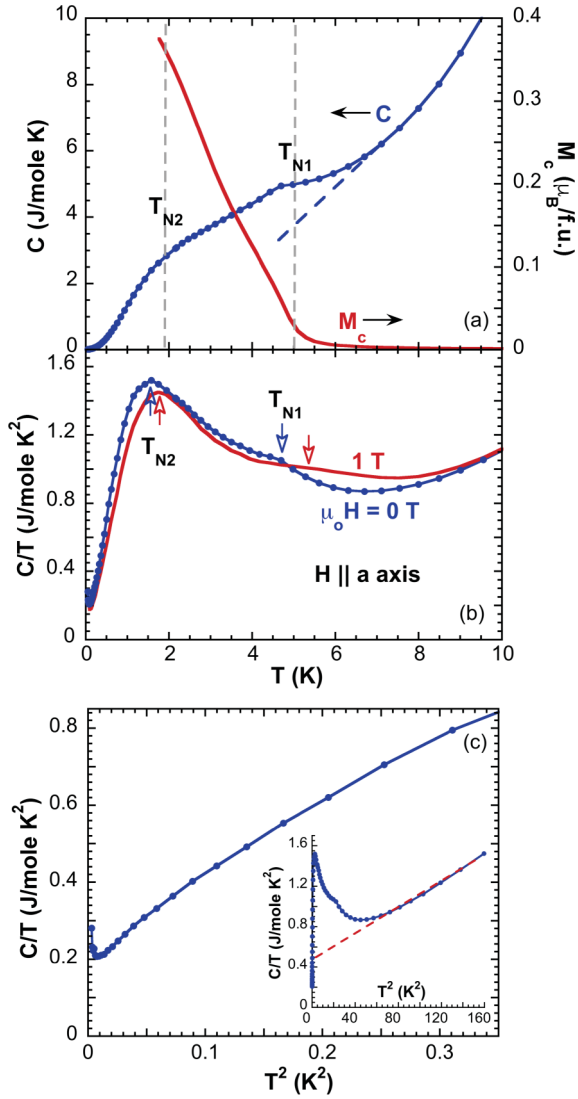

FIG. 3. Heat capacity: Temperature dependence of (a) the specific heat $C(T)$ for a temperature range of 0.05–10 K. M_c in red (right scale) is for comparison. The two gray dashed lines are marks for T_{N1} and T_{N2}; (b) C/T at $\mu_o H = 0$ and 1 T; $H||a$ axis. Note the changes due to the applied field. (c) C/T vs T^2 below 0.6 K; Inset: C/T vs T^2 for $0.05 < T < 12$ K. Note the large interception of the red dashed line on the vertical axis.

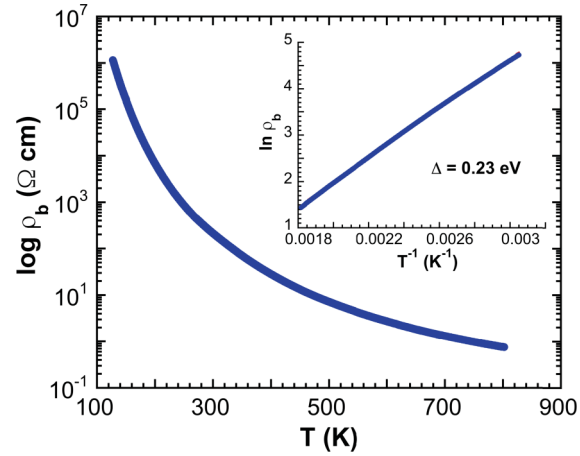

FIG. 4. Temperature dependence of the b-axis electrical resistivity ρ_b. Inset: a fit to the activation law.

them [Fig. 1(a)]. Recent studies have already established that the strong covalency coupled with large SOI within the dimers can be comparable or even stronger than the intra-atomic parameters such as the Hund's rule coupling J_H, forming bonding and antibonding states or molecular orbitals [27–32]. Both Dimer S and Dimer L are apparently the main building blocks of the magnetic state.

$Ba_{13}Ir_6O_{30}$ shares some structural similarities to the dimer-chain system $Ba_5AlIr_2O_{11}$ [27]. The latter iridate features both tetravalent Ir^{4+} and pentavalent Ir^{5+} ions in each of dimers (Ir^{4+}-Ir^{5+} dimer) that are linked via AlO_4 tetrahedra. Despite their one-dimensional character, the dimer chains of $Ba_5AlIr_2O_{11}$ undergo a magnetic order at $T_N = 4.5$ K, remarkably close to $T_{N1} = 4.7$ K, and a charge order at $T_s = 210$ K facilitated by two significantly inequivalent Ir sites [27]. It is found that the magnetic moments are significantly suppressed because of the strong covalency and SOI, which lead to the formation of molecular orbitals [27,28].

This comparison suggests that T_{N1} and the reduced magnetic moments in $Ba_{13}Ir_6O_{30}$ may share the same origin as those in $Ba_5AlIr_2O_{11}$, which, in essence, is a result of the molecular orbitals in the dimers [28]. However, $Ba_{13}Ir_6O_{30}$ exhibits no sign of charge order. Without charge order, an even stronger covalency within each dimer is anticipated, and it favors a fractional occupation of *5d* orbitals in a bonding state. In $Ba_{13}Ir_6O_{30}$, there are six orbitals consisting of two sets of t_{2g} orbitals with a different symmetry in each dimer. Each set of t_{2g} orbitals is split by the strong trigonal distortion into a lower $a1$ orbital and two higher e orbitals. The spatial orientation of these orbitals is such that the $a1$ orbitals form a lower-lying bonding combination and a corresponding higher-lying antibonding orbital $a1^*$ in each dimer. The four e orbitals reside between $a1$ and $a1^*$. The antibonding orbital $a1^*$ is much more energetically costly, in part because the strong SOI pushes it further higher in energy [28]. The splitting between the bonding and antibonding orbitals is thus large, leaving the antibonding orbital $a1^*$ unoccupied [Figs. 5(b) and 5(c)].

The oxidation states in the short and long dimers can be inferred from the associated interatomic distances. The Ir-Ir bond distance in Dimer L is only slightly longer than that of Dimer S by 1.3%. A larger difference (4–5%) would suggest

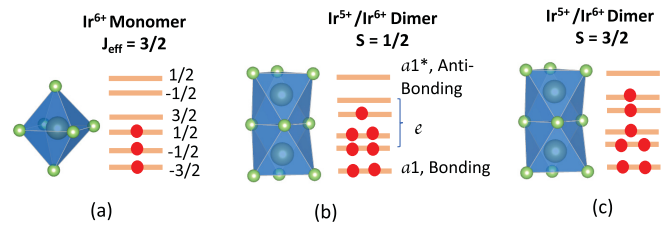

FIG. 5. A sketch for the proposed configurations of orbitals, electrons and total quasispins for (a) the IrO_6 monomer, (b) the Ir^{5+}/Ir^{6+}Dimer with $S = 1/2$, and (c) the Ir^{5+}/Ir^{6+}Dimer with $S = 3/2$.

[24] that the dimers differ in their oxidation state, for example, that Dimer S would host two Ir^{5+} ions and the Dimer L two Ir^{6+} ions (both likely resulting in an effective spin-1 state). While this scenario cannot be ruled out, a likelier scenario is that both Dimers S and L accommodate a mixed oxidation state of Ir^{5+} and Ir^{6+}, thus dimers^{11+}. The strong covalency favors a fractional occupation of *5d* orbitals in a bonding state especially given the strong electron hopping in the dimers [27–30]. The mixed valent state is likely primarily dynamic rather than static since the difference between the two Ir sites in each dimer is very small [33]. A small overlap with the static 5+/6+ configuration could generate electric dipoles in the dimers, which could then alternate the direction in order to minimize the electrical repulsion, as shown in Fig. 1(b). This mostly dynamic mixed valence scenario is consistent with the structural data [33].

There are multiple possible spin states in the dimers^{11+} and the monomers^{6+}. For the monomer, the SOI-entangled $J_{\rm eff} = 3/2$ state is expected [35] [Fig. 5(a)], unless beyond-octahedral distortions become sufficiently strong to quench the spin to a $J_{\rm eff} = 1/2$ state. For the dimers, notice that each of them hosts seven *5d* electrons. The likely possibility is that six of them will doubly occupy the lowest three orbitals and the remaining one electron will singly occupy the next higher orbital, giving rise to a quasispin $S = 1/2$ state [Fig. 5(b)]. A higher spin $S = 3/2$ state is also possible [Fig. 5(c)]; given the observed $\mu_{\rm eff}$, having an effective spin 3/2 state on both dimers and monomers requires an average g factor that is reduced by strong SOI to about $g = 1.15$, which is well within the range of observed g values for ions with high atomic numbers [36]. Therefore, the quasispin 3/2 state for the dimers is a plausible scenario [Fig. 5(c)]. It is emphasized that an effective spin 1/2 state for both the monomer and dimer is inconsistent with the observed $\mu_{\rm eff}$, which is too large for this low-spin scenario, even assuming that the g factors are as large as the bare spin value of $g = 2$. We therefore conclude that at least one site—the monomer, or the dimer, or both—shows a large effective spin 3/2 state.

The large-spin state(s) across two distinct magnetic sites produces a large number of degrees of freedom ($2S + 1$ each), which should explain the striking features, namely (1) ferrimagnetism, i.e., antiferromagnetic correlations with a coincident nonzero net ferromagnetic moment [Fig. 2(c)] (2) a magnetic transition followed by a distinct crossover-like feature at a lower temperature [Figs. 2(a) and 3(a)], and (3) huge low-temperature entropy $\gamma = 200\,{\rm mJ/mole\,K^2}$ [Fig. 3(c)]. A ferrimagnetic order is required by the negative (antiferromagnetic) Curie-Weiss temperatures [Fig. 2(b) inset] together with the hysteresis seen below $T_{\rm N1}$ and its associated net ferromagnetic moment. Ferrimagnetism is generically expected due to the presence of two distinct magnetic sites, and in this case, the monomers and dimers. The $T_{\rm N2}$ crossover and the large residual entropy that remains even below $T_{\rm N2}$ suggest that the ordering preserves residual entropy in the form of unquenched degrees of freedom or numerous low energy excitations. This is consistent with the geometric frustration due to the complicated multisite lattice and the frustration from competition of exchange interactions and single-ion anisotropy (which arises since at least one magnetic site hosts an effective spin 3/2 state): the competition among these interactions that generically prevents any single classical configuration from having much lower energy than all others (i.e., the magnetic frustration) generically leads to emergent low energy scales and associated low energy degrees of freedom [37].

$J_{\rm eff} = 3/2$ iridates with the complex interplay of correlations and SOI have been largely unexplored, and so far there is insufficient information to determine the magnetic order here. We can, however, point out a few possibilities that are consistent with the available experimental data: (A) collinear ferrimagnetic order with different moments on dimers and monomers that undergoes a second crossover into a more complicated state, either with unusual quantum correlations or, e.g., classical noncollinear canting; or (B) a noncollinear order with a small net ferromagnetic moment, of which the paradigmatic well-known example is a skyrmion crystal magnetic texture. Skyrmions and related small-net-moment antiferromagnetic textures [38] are known to be able to arise from various related mechanisms based on SOI, including (i) competition between single-ion spin anisotropy of large spin (greater than spin half) and antisymmetric DM interactions; and (ii) magnetic frustration in large-spin magnets with strong SOI [39,40]. Both mechanisms suit the present setting of the spin 3/2 state arising from strong SOI: Mechanism (i) requires DM interactions, which are allowed due to the absence of inversion symmetry on lines connecting dimers, associated with the low symmetry configuration of octahedral dimers; while the magnetic frustration of Mechanism (ii) arises naturally from the lattice formed by the multiple magnetic sites (monomers and short and long dimers). Interestingly, Mechanism (ii), which is likely the primary mechanism, would result in a dense skyrmion lattice, with the skyrmion-lattice-scale related to the microscopic crystal scale by a factor of order one. A skyrmion lattice is an especially appealing theoretical scenario for explaining the measurements if $T_{\rm N2}$ is interpreted as a weak transition rather than just a short ranged feature: in addition to its ferrimagnetism, and its gapless phonons and other low energy modes with residual entropy, it is distinguished from other frustrated ferrimagnets in that it can easily produce a second instability at a lower temperature $T_{\rm N2}$.

III. CONCLUSIONS

The large γ remains the most surprising and intriguing experimental feature of this compound. Indeed, the value of γ is nearly zero for the dimer-chain $Ba_5AlIr_2O_{11}$ that features a quasispin $S = 1/2$ state [28], although it similarly orders at $T_{\rm N} = 4.5\,{\rm K}$ [27]. A full characterization of the lowest temperature magnetic order may help shed light on this striking feature. We expect that the key ingredient for the large quantum entropy at low temperatures, as for the other striking experimental observations here, relies on the unusually large spin degrees of freedom unique to the structure of this iridate and, in particular, its monomers and dimers of Ir^{6+} ($5d^3$) ions. All in all, this work provides a paradigm for discovery and study of quantum states in spin-orbit-entangled, high-spin materials, which have remained largely unexplored.

ACKNOWLEDGMENTS

This work was supported by the National Science Foundation via Grants No. DMR-1712101 and No. DMR 1903888. I.K. was supported by a National Research Council Fellowship through the National Institute of Standards and Technology. We thank Professor Arun Paramekanti for a discussion of his work on skyrmion crystals.

[1] B. J. Kim, H. Jin, S. J. Moon, J. Y. Kim, B. G. Park, C. S. Leem, J. Yu, T. W. Noh, C. Kim, S. J. Oh, J. H. Park, V. Durairaj, G. Cao, and E. Rotenberg, Novel $J_{\rm eff} = 1/2$ Mott State Induced by Relativistic Spin-Orbit Coupling in Sr_2IrO_4, Phys. Rev. Lett. **101**, 076402 (2008).

[2] S. J. Moon, H. Jin, K. W. Kim, W. S. Choi, Y. S. Lee, J. Yu, G. Cao, A. Sumi, H. Funakubo, C. Bernhard, and T. W. Noh, Dimensionality-Controlled Insulator-Metal Transition and Correlated Metallic State in 5*d* Transition Metal Oxides $Sr_{n+1}Ir_nO_{3n+1}$ ($n = 1$, 2, and ∞), Phys. Rev. Lett. **101**, 226402 (2008).

[3] B. J. Kim, H. Ohsumi, T. Komesu, S. Sakai, T. Morita, H. Takagi, and T. Arima, Phase-sensitive observation of a spin-orbital mott state in Sr_2IrO_4, Science **323**, 1329 (2009).

[4] G. Jackeli and G. Khaliullin, Mott Insulators in the Strong Spin-Orbit Coupling Limit: From Heisenberg to a Quantum Compass and Kitaev Models, Phys. Rev. Lett. **102**, 017205 (2009).

[5] W. Witczak-Krempa, G. Chen, Y. B. Kim, and L. Balents, Correlated quantum phenomena in the strong spin-orbit regime, Annu. Rev. Condens. Matter Phys. **5**, 57 (2014).

[6] J. G. Rau, E. K. H. Lee, and H. Y. Kee, Spin-orbit physics giving rise to novel phases in correlated systems: Iridates and related materials, Annu. Rev. Condens. Matter Phys. **7**, 195 (2016).

[7] G. Cao and P. Schlottmann, The challenge of spin-orbit-tuned ground states in iridates: A key issues review, Rep. Prog. Phys. **81**, 042502 (2018).

[8] M. Hermanns, I. Kimchi, and J. Knolle, Physics of the Kitaev model: Fractionalization, dynamic correlations, and material connections, Annu. Rev. Condens. Matter Phys. **9**, 17 (2018).

[9] G. Cao, T. F. Qi, L. Li, J. Terzic, S. J. Yuan, L. E. DeLong, G. Murthy, and R. K. Kaul, Novel Magnetism of $Ir^{5+}(5d^4)$ Ions in the Double Perovskite Sr_2YIrO_6, Phys. Rev. Lett. **112**, 056402 (2014).

[10] J. Terzic, H. Zheng, Feng Ye, P. Schlottmann, H. D. Zhao, L. DeLong, S. J. Yuan, and G. Cao, Evidence for a low-temperature magnetic ground state in double-perovskite iridates with $Ir^{5+}(5d^4)$ ions, Phys. Rev. B **96**, 064436 (2017).

[11] G. Khaliullin, Excitonic Magnetism in Van Vleck-Type d^4 Mott Insulators, Phys. Rev. Lett. **111**, 197201 (2013).

[12] O. N. Meetei, W. S. Cole, M. Randeria, and N. Trivedi, Novel magnetic state in d^4 Mott insulators, Phys. Rev. B **91**, 054412 (2015).

[13] S. Bhowal, S. Baidya, I. Dasgupta, and T. Saha-Dasgupta, Breakdown of $\mathbf{J} = 0$ nonmagnetic state in d^4 iridate double perovskites: A first-principles study, Phys. Rev. B **92**, 121113(R) (2015).

[14] A. J. Kim, H. O. Jeschke, P. Werner, and R. Valenti, **J** Freezing and Hund's Rules in Spin-Orbit-Coupled Multiorbital Hubbard Models, Phys. Rev. Lett. **118**, 086401 (2017).

[15] C. Svoboda, M. Randeria, and N. Trivedi, Effective magnetic interactions in spin-orbit coupled d^4 Mott insulators, Phys. Rev. B **95**, 014409 (2017).

[16] J.-H. Choy, D.-K. Kim, S.-H. Hwang, G. Demazeau, and D.-Y. Jung, XANES and EXAFS studies on the Ir-O bond covalency in ionic iridium perovskites, J. Am. Chem. Soc. **117**, 8557 (1995).

[17] S.-J. Kim, M. D. Smith, J. Darriet, and H.-C. zur Loye, Crystal growth of new perovskite and perovskite related iridates: $Ba_3LiIr_2O_9$, $Ba_3NaIr_2O_9$, and $Ba_{3.44}K_{1.56}Ir_2O_{10}$, J. Solid State Chem. **177**, 1493 (2004).

[18] H.-C. zur Loye, S.-J. Kim, R. Macquart, M. D. Smith, Y. Lee, and T. Vogt, Low temperature structural phase transition of $Ba_3NaIr_2O_9$, Solid State Sci. **11**, 608 (2009).

[19] P. Kayser, M. J. Martínez-Lope, J. A. Alonso, M. Retuerto, M. Croft, A. Ignatov, and M. T. Fernández-Díaz, Crystal structure, phase transitions, and magnetic properties of iridium perovskite Sr_2MIrO_6 (M = Ni, Zn), Inorg. Chem. **52**, 11013 (2013).

[20] L. Yang, A. Pisoni, A. Magrez, S. Katrych, A. Arakcheeva, B. Dalla Piazza, K. Prša, J. Jaćimović, A. Akrap, J. Teyssier, L. Forró, and H. M. Rønnow, Crystal structure, transport, and magnetic properties of an Ir^{6+} compound $Ba_8A_{12}IrO_{14}$, Inorg. Chem. **54**, 4371 (2015).

[21] S. Vasala, H. Yamauchi, and M. Karppinen, Synthesis, crystal structure and magnetic properties of a new B-site ordered double perovskite Sr_2CuIrO_6, J. Solid State Chem. **220**, 28 (2014).

[22] J. Park, J.-G. Park, I. P. Swainson, H.-C. Ri, Y. N. Choi, C. Lee, and D.-Y. Jung, Neutron diffraction studies of $Ba_2CaIr(VI)O_6$, J. Korean Phys. Soc. **41**, 118 (2002).

[23] G. Demazeau, D.-Y. Jung, J.-P. Sanchez, E. Colineau, A. Blaise, and L. Fournes, Iridium(VI) stabilized in a perovskite-type lattice: Ba_2CaIrO_6, Solid State Commun. **85**, 479 (1993).

[24] T. Sakamoto, Y. Doi, and Y. Hinatsu, Crystal structures and magnetic properties of 6H-perovskite-type oxides $Ba_3MIr_2O_9$ (M = Mg, Ca, Sc, Ti, Zn, Sr, Zr, Cd and In), J. Solid State Chem. **179**, 2595 (2006).

[25] M. A. Laguna-Marco, P. Kayser, J. A. Alonso, M. J. Martínez-Lope, M. van Veenendaal, Y. Choi, and D. Haskel, Electronic structure, local magnetism, and spin-orbit effects of Ir(IV)-, Ir(V)-and Ir(VI)-based compounds, Phys. Rev. B **91**, 214433 (2015).

[26] A. E. Taylor, S. Calder, R. Morrow, H. L. Feng, M. H. Upton, M. D. Lumsden, K. Yamaura, P. M. Woodward, and A. D. Christianson, Spin-Orbit Coupling Controlled $J_{\rm eff} = 3/2$ Electronic Ground State in $5d^3$ Oxides, Phys. Rev. Lett. **118**, 207202 (2017).

[27] J. Terzic, J. C. Wang, Feng Ye, W. H. Song, S. J. Yuan, S. Aswartham, L. E. DeLong, S. V. Streltsov, D. I. Khomskii, and G. Cao, Coexisting charge and magnetic orders in the dimer-chain iridate $Ba_5AlIr_2O_{11}$, Phys. Rev. B **91**, 235147 (2015).

[28] S. V. Streltsov, G. Cao, and D. I. Khomskii, Suppression of magnetism in $Ba_5AlIr_2O_{11}$: Interplay of Hund's coupling, molecular orbitals and spin-orbit interaction, Phys. Rev. B **96**, 014434 (2017).

[29] M. Ye, H.-S. Kim, J.-W. Kim, C.-J. Won, K. Haule, D. Vanderbilt, S.-W. Cheong, and G. Blumberg, Covalency-driven collapse of strong spin-orbit coupling in face-sharing iridium octahedra, Phys. Rev. B **98**, 201105(R) (2018).

[30] Y. Wang, R. Wang, J. Kim, M. H. Upton, D. Casa, T. Gog, G. Cao, J. P. Hill, G. Kotliar, M. P. M. Dean, and X. Liu, Direct Detection of Dimer Orbitals in $Ba_5AlIr_2O_{11}$, Phys. Rev. Lett. **122**, 106401 (2019).

[31] G. Cao, H. D. Zhao, H. Zheng, Y. F. Ni, C. A. Pocs, Y. Zhang, F. Ye, C. Hoffmann, X. Wang, M. Lee, M. Hermele, and I. Kimchi, Quantum liquid from strange frustration in the trimer magnet $Ba_4Ir_3O_{10}$, arXiv:1901.04125.

[32] L. Xu, R. Yadav, V. Yushankhai, L. Siurakshina, J. van den Brink, and L. Hozoi, Superexchange interactions between spin-orbit-coupled $j \approx 1/2$ ions in oxides with face-sharing ligand octahedra, Phys. Rev. B **99**, 115119 (2019).

[33] See Supplemental Material at http://link.aps.org/supplemental/10.1103/PhysRevB.100.064418 for details of the crystal structure and experimental techniques.

[34] O. B. Korneta, S. Chikara, L.E. DeLong, P. Schlottmann, and G. Cao, Pressure-induced insulating state in single-crystal $Ba_{1-x}Gd_xIrO_3$, Phys. Rev. B **81**, 045101 (2010).

[35] S. V. Streltsov and D. I. Khomskii, Orbital physics in transition metal compounds: New trends, Phys. Usp. **60**, 1121 (2017).

[36] Pascal Quinet and Emile Biémont, Landé g factors for experimentally determined energy levels in doubly ionized lanthanides, At. Data Nucl. Data Tables. **87**, 207 (2004).

[37] L. Balents, Spin liquids in frustrated magnets, Nature (London) **464**, 199 (2010).

[38] S. Mühlbauer, B. Binz, F. Jonietz, C. Pfleiderer, A. Rosch, A. Neubauer, R. Georgii, and P. Böni, Skyrmion lattice in a chiral magnet, Science **323**, 915 (2009).

[39] A. Bogdanov and A. Hubert, Thermodynamically stable magnetic vortex states in magnetic crystals, J. Magn. Magn. Mater. **138**, 255 (1994).

[40] V. Lohani, C. Hickey, and A. Rosch, Quantum skyrmions in frustrated ferromagnets, arXiv:1901.03343.